Novel Software-based Method to Widen Dynamic Range of CCD Sensor Images

Wei Wen, Siamak Khatibi

Department of Communication System, Blekinge technical Institute, Karlskrona, Sweden
{wei.wen, siamak.khatibi}@bth.se

Abstract. In the past twenty years, CCD sensor technology has made significant progress in increasing resolution and improving low-light performance by hardware. However due to physical limits of the sensor design and fabrication, fill factor has become the bottle neck problem for improving quantum efficiency of CCD sensor in order to widen dynamic range of output image. In this paper we propose a novel software-based method to compensate the performance degradation of the dynamic range, by virtual increase of fill factor which is achieved by a resampling process. In our method, the CCD sensor images are rearranged to a new grid of virtual sensor pixels, each of which is composed by subpixels. A statistical framework consisting of local learning model, simulations and Bayesian inference is used to estimate new subpixel intensity values. The highest probability of sub-pixels intensity values in each resampled pixel area is used to estimate the pixel intensity values of a new dynamic range enhanced image.

From generation of gray level optical images, CCD images with different fill factors were obtained. By knowing the fill factor and having the CCD image, a new resampled image was computed. Each resampled image was compared to the respective CCD and optical image. The results of such comparison show that by using the proposed method it is possible to widen significantly the recordable dynamic range of CCD images and obtain a virtual increase of fill factor to 100%. The stability and fill factor dependency of the proposed method were also examined in which the results showed insignificant spreading effect and fill factor dependency.

Keywords: dynamic range, fill factor, CCD sensors, sensitive area, quantum efficiency

1 Introduction

Since the first digital cameras equipped with charge-coupled device (CCD) image sensors in 1975 [1] the investigation on human visual system has been affecting the digital camera design and their development. In human visual system the retina, formed by the rod and cone photoreceptors, initiates the visual process by converting a continuous image to a discrete array of signals. Curcio et el. [2] investigation on human photoreceptor revealed that the properties of the rods and cones mosaic deter-

mine the amount of information which is retained or lost by sampling process, including resolution acuity and detection acuity. The photoreceptor layer specialized for maximum visual acuity is in the center of the retina, the fovea, which is 1.5 mm wide and is composed by cones entirely. Fig.1 shows a close up of the fovea region. The shape of cones is much closed to hexagonal and the cones in fovea are densely packed, where no gap between each two cones can be considered. Due to this configuration the visual acuity and neural sampling in fovea are optimized [3].

The image sensor array in a CCD digital camera is designed by modelling the fovea in human eyes for capturing and converting the analog optical signal from a scene into a digital electrical signal. Over the past twenty years, the quality of digital camera sensors has made tremendous progress, especially in increasing resolution and improving low-light performance [4]. This has been achieved by reducing the pixel size and improving the quantum efficiency (QE) of the sensor [4, 5]. Assuming each pixel corresponding to one cone in fovea, the pixel density in camera sensor should be close to 199,000 /mm2 which is the average density of the peak fovea cones in human eyes [2]. Todays the pixel density can be 24,305 /mm2 in a common commercial camera such as Canon EOS 5D Mark II or the pixel density can be even higher as 480,000/mm2 in a special camera such as Nokia 808. However the quality of the image is not affected only by the pixel size or quantum efficiency of the sensor [6]. As the sensor pixel size becomes smaller this results to detect a smaller die size, gain higher spatial resolution and obtain lower signal-to-noise ratio (SNR); all in cost of lower recordable dynamic range (DR) and lower fill factor (FF). Hardware solutions in image sensor technologies as a respond to increase of mobile imaging applications try to compensate for the performance degradation with decrease of the pixel size. On the other hand the only standard post-processing solution for obtaining a nearly infinite displayable dynamic range is to use the high dynamic range imaging technology which implements a combination of several images captured with different exposure times or different sizes of aperture sensor [7, 8].

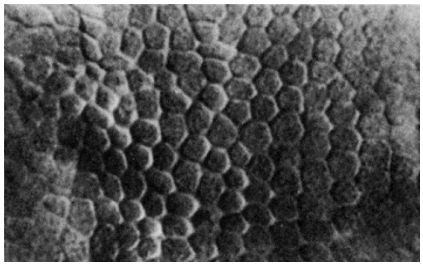

Fig. 1. A close up of the fovea region [2].

In this paper we propose a novel software-based method to compensate the performance degradation of the recordable dynamic range, with decrease of the pixel size, by virtual increase of fill factor. In our method the original fill factor is known and the processing is done on the captured image. The virtual increase of fill factor is achieved by a statistical resampling process which initiates the estimation of each new pixel intensity value. Our results show that it is possible to widen the dynamic range

significantly by software solution. Although there are software technologies to improve the displayable dynamic range using only one image, such as the histogram equalization and image contrast enhancement [9], to the best of our knowledge, our approach is the first work that tries to improve the recordable dynamic range by virtually increase of the fill factor of a CCD sensor.

The rest of paper is organized as follow; in section 2 the effect of fill factor is explained, in section 3 the details of the method are described, section 4 explains the experimental setup, the results are shown and discussed in section5, and finally we conclude and discuss potential future work in section 6. Here it is worth to mention that we distinguish between recordable and displayable dynamic range where the recordable dynamic range represents the raw input dynamic range obtained after capturing of an image and the displayable dynamic range is considered a post-processing operation on the raw captured image.

2 Effect of fill factor

CCD sensor has reigned supreme in the realm of imaging with the steady improvement of performance, especially on scientific area [5] due to its advantage of high quantum efficiency. The QE which is defined as the number of signal electrons created per incident photon is one of the most important parameters used to evaluate the quality of a detector which affects the DR and SNR of captured images. Fig. 2 is the graphical representation of a CCD sensor showing some buckets and rain drops shown as blue lines. Each bucket represents storage of photoelectrons, by modelling a photodiode and a well of one pixel in the CCD sensor and the rain drops, blue lines, represent the incident photons that fall into the sensor. By having bigger bucket more rain drops, number of photons, is collected, which can be seen as increase of the spatial quantum efficiency [10] resulting in DR quality improvement of captured images. The temporal quantum efficiency is related to accumulation of photoelectrons during the exposure time and is regulated by the fill factor [5].

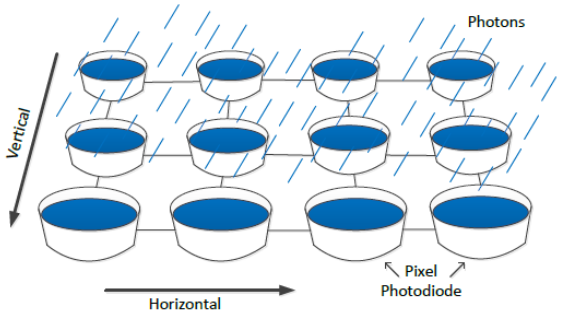

Fig. 2. Graphical representation of a CCD sensor.

The quantum efficiency is affected by fill factor as in $QE_{eff} = FF \times QE$, where QE_{eff} is the effective QE and FF is the fill factor which is the ratio of light sensitive

area versus total area of a pixel [5]. A typical dynamic range, the ratio of the brightest accurately detectable signal to the faintest, of CCD sensors is proportional to the number of detected photons. The fill factor of non-modified CCD sensor varies from 30% to 75%. Fig. 3(a) and 3(b) show light incident on a sensor with high and low fill factor pixels respectively. In a sensor with the high fill factor pixels more number of photons is captured in comparison to a sensor with the low fill factor pixels. Hardware innovations in image sensor technologies (e.g. decrease of occupied area of the pixel transistors, increase of the photodiode area within maintaining small pixel size and use of microlenses) are achieved to increase the fill factor. An effective way to increase the fill factor is to put a microlens above each pixel which converges light from the whole pixel unit area into the photodiode in order to capture more number of photons as shown in Fig. 3(c). Since 90s, various microlens have been developed for increasing fill factor and they are widely used in CCD sensors [12, 13]. But it is still impossible to make fill factor 100% in practical production due to the physical limits in digital camera development [4]. Our proposed method compensates the loss of input signal, caused by incident light on non-sensitive area, in each sensor pixel to achieve a fill factor of 100%.

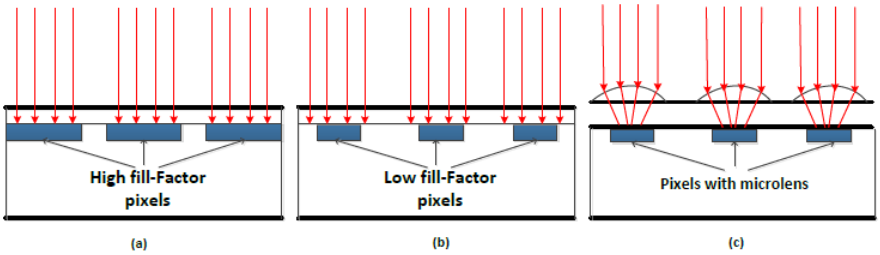

Fig. 3. Light incident on sensor with high and low fill factor pixels are shown in (a) and (b) respectively. (c) Pixel with the micro-lens is used to compensate the entering light. [11]

3 Methodology

By collecting incoming photons into a sample grid, a CCD sensor samples an image. Fig. 4 illustrates such conventional sampling grid on a CCD sensor array of four pixels. The white and black areas represent the sensitive areas and non-sensitive areas in pixels respectively. The blue arrows in the figure represent the positions of sampled signal. Let assume the size of each pixel is Δx by Δy. Then Δx and Δy , the sample interval in x and y directions, are the spatial resolution of the output image. The sampling function can be expressed as $F(x', y') = \sum_{i=0}^{M} \sum_{j=0}^{N} \delta(i\Delta x, j\Delta y) f(x, y)$ where x, y, x' and y' are pixel coordinates in the input optical image f and the output sampled image F , with size of M by N, respectively [14]. Let also assume the size of the sensitive area is $\Delta x'$ by $\Delta y'$ as shown in Fig. 4. Thus when the incident light is not in the sensitive area with size of $\Delta x'$ by $\Delta y'$, $F(x', y') = 0$.

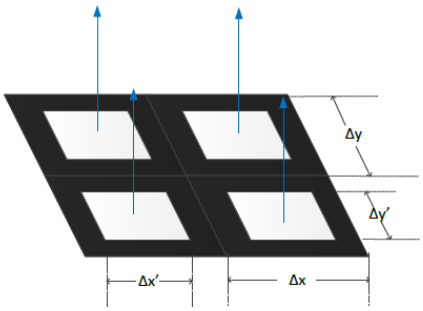

Fig. 4. The conventional image sampling on a CCD sensor.

Based on the discussion in Section 2 the fill factor is lower than 100%, in that case the region of support corresponding to the sensitive area is not the whole area of one pixel. A signal resampling procedure is used in order to expand the region of support and improve the captured signal. For each pixel the resampled procedure consists of following parts: a) local learning model, b) sub-pixel rearrangement, c) model simulations on sub-pixel grid, d) intensity estimating of sub-pixels based on Bayesian inference, and e) pixel intensity estimation based on highest probability. Each part of the procedure is explained in more details as it follows.

a) **Local learning model** – In a neighborhood of the actual pixel one or combination of several statistical models are tuned according to data structure in the neighborhood. We used a Gaussian statistical model in our experiments.

b) **Sub-pixel rearrangement** - By knowing the fill factor, the CCD image is rearranged in a new grid of virtual sensor pixels, each of which consisting of virtual sensitive and non-sensitive areas. Each of these areas is defined by integer number of sub-pixels. The intensity value of each pixel in the CCD image is assigned to all of sub-pixels in the virtual sensitive area. The intensity values of all sub-pixels in non-sensitive area in virtual sensor pixels were assigned to zero. An example of such rearrangement of sampled data to sub-pixel level is presented in section 4.

c) **Model simulations on sub-pixel grid** – In a sub-pixel rearranged neighborhood of the actual pixel, the local learned model is used to simulate all intensity values of the sub-pixels. The known intensity values of virtual sensitive sub-pixels and result of linear interpolation on the sub-pixel grid for obtaining the unknown intensity values of virtual non-sensitive sub-pixels are used to initiate the intensity values in the simulation. Several simulations are accomplished where in each one the number of actual sub-pixels varies from zeros to total number of sub-pixels of the actual virtual sensitive area. In this way each sub-pixel of the actual virtual sensor obtains, after a number of simulations, various random intensity values.

d) **Intensity estimating of sub-pixels based on Bayesian inference** – Bayesian inference is employed to estimate the intensity of each sub-pixel by having the model

simulations values as the observation values. Let y be the observed intensity value of each sub-pixel after simulations and x be the true intensity value of the sub-pixel, then

$$y = x + n$$

where n can be considered as the contaminated noise by the linear interpolation process. Here the goal is to make the best guess, $\hat{x}$, of the value x given the observed values by

$$\hat{x} = \arg\max_x P(x|y),$$

$$\text{and} \quad P(x|y) = \frac{P(y|x)P(x)}{P(y)}$$

where P(x|y) is the probability distribution of x given y, P(y|x) is the probability distribution of y given x, P(x) and P(y) are the probability distribution of x and y.

By assumption of having a Gaussian noise yields

$$P(y|x) = \mathrm{P}(x|x+n) = \frac{1}{\sqrt{2\pi}\sigma_n} e^{-\frac{(y-x)^2}{2\sigma_n^2}}$$

where σ_n is the variance of the noise; i.e. the variance of interpolated data from simulations for each sub-pixel . The educated hypothesis P(x) is obtained by the local learning model which here has a Gaussian distribution with the mean μ_x and standard deviation of σ_x as following

$$\mathrm{P}(x) = \frac{1}{\sqrt{2\pi}\sigma_x} e^{-\frac{(\mathrm{x}-\mu_x)^2}{2\sigma_x^2}}$$

For posterior probability on x yields

$$P(x|y) \approx P(y|x)\mathrm{P}(x) = \frac{1}{\sqrt{2\pi}\sigma_n} e^{-\frac{(y-x)^2}{2\sigma_n^2}} \times \frac{1}{\sqrt{2\pi}\sigma_x} e^{-\frac{(\mathrm{x}-\mu_x)^2}{2\sigma_x^2}}$$

The x which maximizes P(x|y) is the same as that which minimizes the exponent term in the above equation. Thus if $\mathrm{f}(x) = -\frac{(y-x)^2}{2\sigma_n^2} - \frac{(\mathrm{x}-\mu_x)^2}{2\sigma_x^2}$, when the derivative $\mathrm{f}'(x) = 0$, the minimum value or the best intensity estimation of the corresponding subpixel is

$$\hat{x} = \frac{y\sigma_x^2 + \mu_x\sigma_n^2}{\sigma_x^2 + \sigma_n^2}$$

e) **Pixel intensity estimation based on highest probability** – The histogram of intensity values of the actual virtual sensor sub-pixels is calculated which indicates a tendency of intensities probability. The multiplication of inverse of fill factor with

highest value of such probability is considered as the estimated intensity value of the actual virtual sensor as the result of resampling procedure.

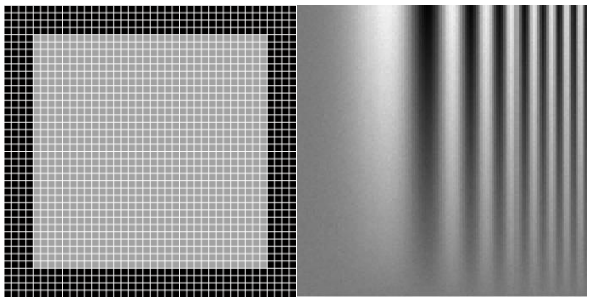

Fig. 5. The virtual CCD image sensor pixel composed by subpixels whose fill factor is set as 81% (left) and the optical image (right).

4 Experimental setup

Several optical and CCD images for different fill factor values were simulated using our own codes and Image Systems Evaluation Toolbox (ISET) [15] in MATLAB. ISET is designed to evaluate how image capture components and algorithms influence image quality, and has been proved to be an effective tool for simulating the sensor and image capturing [16]. Five fill factor values of 25%, 36%, 49%, 64% and 81%, were chosen for five simulated CCD sensors, having the same resolution of 128 by 128. All sensors had a pixel area of 10 by 10 square microns, with well capacity of 10000 e-. The read noise and the dark current noise were set to 1 mV and 1 mV/pixel/sec respectively. Each CCD sensor was rearranged to a new grid of virtual sensor pixels, each of which was composed of 40-by-40 sub-pixels. Fig. 5 shows an example of the rearranged CCD sensor pixel with fill factor value of 81%. The light grey and the dark grey areas represent the sensitive and the non-sensitive areas respectively. The sensitive area in each pixel was located in the middle of each pixel. The intensity value of subpixels in the virtual sensitive area was assigned by correspondent output image pixel intensity. The intensity values of all sub-pixels in non-sensitive area were assigned to zero. One type of optical and sensor image were generated and called as sweep frequency image. The intensity values of the sweep frequency image were calculated, in each row, from a linear swept –frequency cosine function. For generation of CCD sensor images, the luminance of the sweep frequency image was set to 100 cd/m^2 and the diffraction of the optic system was considered limited to ensure to obtain the brightness of the output as close as possible to the brightness of scene image. The exposure time was also set to 0.9 ms for all simulated five sensors to ensure constant number of input photons in the simulations.

5 Results and discussion

The conventional sampled images from the sweep frequency optical images are shown in the first row of Fig. 6, the second row of images show the resampled images with our method. The result images from histogram equalization and image enhancement methods are shown in the third and fourth rows. The images of each row are related to different fill factor values, which are 25%, 36%, 49%, 64% and 81% from left to right. All the images in Fig. 6 are displayed in unsigned 8 bits integer (uint8) format without any DR normalization. It can be seen that the DR of the conventional sampled images are very different from each other. When the fill factor is increasing, the DR is increased as well and approaching to the DR level of optical image shown in the Fig. 5. This is according to proportional relation of fill factor to number of photons which results to the intensity value changes of each pixel. The appearance of all resampled images with our proposed method is shown in Fig. 6 respectively. The top row of each image related to the sweep frequency optical image is chosen to visualize a typical comparison of pixel intensity values in these images. Fig. 7 shows such pixel intensity values from conventional sampled images with the label of fill factor (FF) percentage, the optical and the resampled image from the image of 25% fill factor with our method. The results in Fig. 7 are consistent with the image appearance in Fig. 6. These also verify that the pixel intensity values are increased as a consequence of virtual increase of fill factor by our method.

The dynamic range and root mean square error (RMSE) are used for comparison of the conventional sampled images, our resampled images and the respective optical image. The dynamic range is calculated by $DR = 20 \times \log_{10} p_{max}/p_{min}$, where p_{max} and p_{min} are the maximum and minimum pixel intensity values in an image. In uint8, there are 256 grey levels, which it means the maximum DR is 48.13 based on the above equation. The RMSE is defined as

$$RMSE = \sqrt{\frac{1}{n}\sum_{i=1}^{n}(P_i - Q_i)^2}$$

where P_i and Q_i are the intensities of correspondent pixels in two compared images, and n is the number of pixels. The DR, RMSE and entropy results for the sweep frequency related images are shown in Table 1 and 2 respectively, where the entropy of an image is used to evaluate the amount of information preservation after implementation of each method. Generally when the fill factor is increasing, the RMSEs between the optical image and the other images are decreasing, on the contrary entropy values and DRs are increasing. The tables also show that our method not only widen DRs in comparison to the conventional method but also preserve the information, shown in entropy values, and approach the truth data of the optical image, shown in RMSEs values, significantly better than post-processing solutions of histogram equalization and image contrast enhancement methods.

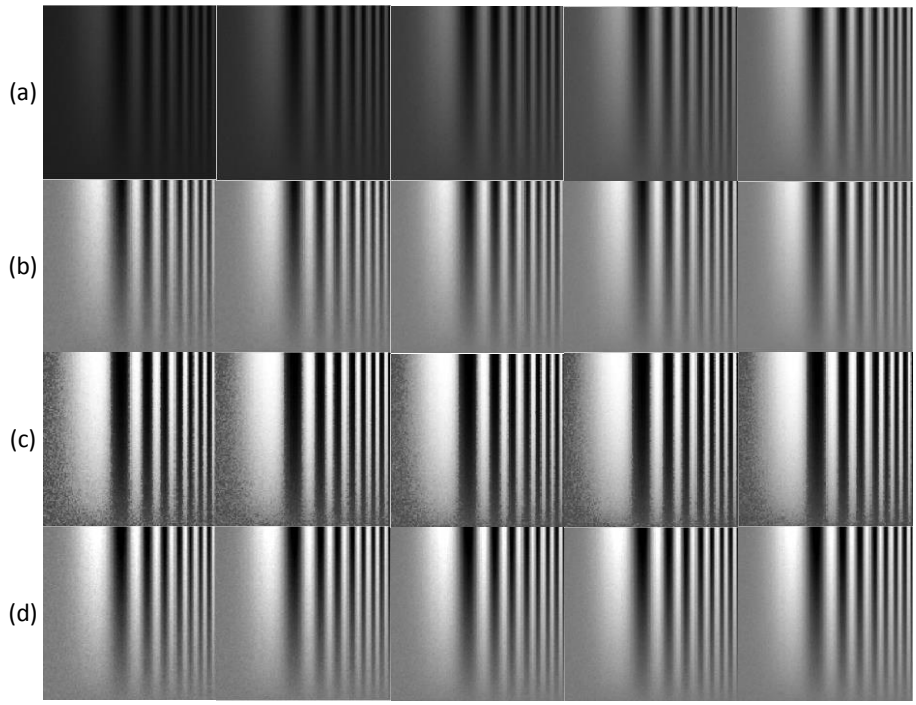

Fig. 6. The conventional sampled images (a) from the sweep frequency optical image having different fill factors, and the resampled image with our method (b), and the result images from histogram equalization (c) and image contrast enhancement (d). From left to right, the sensor fill factors are 25%, 36%, 49%, 64% and 81%.

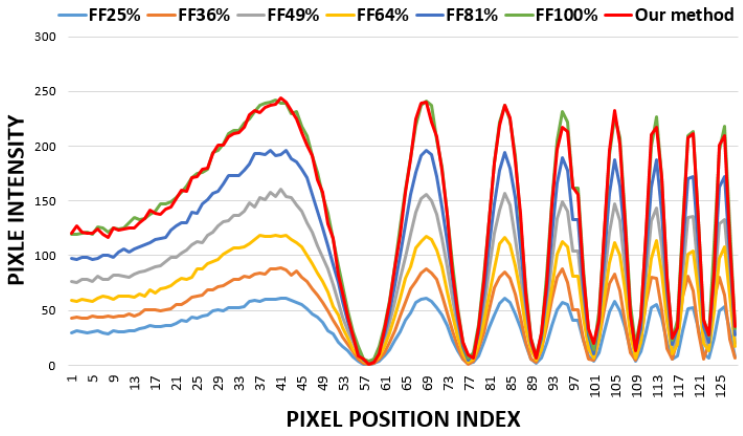

Fig. 7. The row wise comparison of pixel intensity values in sweep frequency related images.

Table 1. The RMSE and dynamic range (DR in dB) comparison between the optical image and the result images related to different methods having different fill factor (FF) percentage.

Methods	FF25%		FF36%		FF49%		FF64%		FF81%		Mean
	RMSE	DR	RMSE	DR	RMSE	DR	RMSE	DR	RMSE	DR	RMSE
Conventional method	102.54	36	87.51	39	69.5	42	49.63	44	26.4	46	67.16
Our method	4.69	48	9.79	48	3.6	48	3.09	48	2.79	48	4.79
Histogram Equalization	36.24	48	38.13	48	36.13	48	36.25	48	36.11	48	36.57
Image Contrast enhancement	12.08	48	14.84	48	11.39	48	10.95	48	10.87	48	12.03

Table 2. The Entropy comparison between the optical image and the result images related to different methods having different fill factor (FF) percentage.

Methods	FF25%	FF36%	FF49%	FF64%	FF81%	Standard deviation
Conventional method	5.34	5.90	6.29	6.67	7.00	0.64
Our method	7.31	7.35	7.33	7.33	7.33	0.02
Histogram Equalization	5.1	5.42	5.59	5.77	5.80	0.27
Image Contrast enhancement	5.28	5.84	6.22	6.64	6.92	0.64

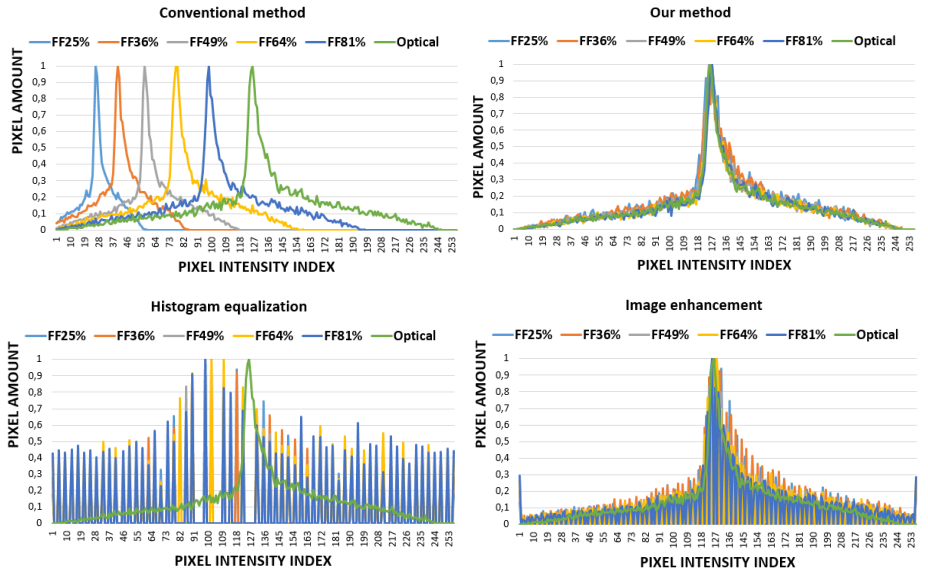

Fig. 8. The normalized histogram envelopes of conventional sampled images related to the sweep frequency optical image and correspondent our proposed resampled images, the images created with histogram equalization and image contrast enhancement.

Fig. 8 shows the histograms envelopes of the conventional sampled images and the resampled images by our method and another two post-processing methods for improving the dynamic range. The results in the figures verify as well our statement that the dynamic range is widening by our method. The top left plot in Fig. 8 shows the histogram envelopes of the conventional sampled images and the truth optical image. The dynamic range varies with the change of fill factor for the conventional sampled images and by increase of fill factor the width of dynamic range is also increased. However the histogram envelopes of the resampled images by our method, shown in top right plot in Fig. 8, have the same width of dynamic range, independent of fill factor changes, and the DR is significantly close to DR of the truth optical image. The histograms envelopes of images by the post-processing methods, shown in bottom left plot in Fig. 8, have wider range than the conventional method, but fewer numbers of gray level indexes in comparison to our method, which is also consistent with result of the entropy in Table 2 indicating unsuccessfulness of such methods in preservation of information. The obtained results from the resampling images by our method show that the dependency of the method to fill factor is not significant, see Table 3. In the table the standard deviation of the histograms of result images by different methods are presented which indicating three issues: first the changes in the standard deviation of histograms are correlated to the preservation of original information, see the Table 2; secondly our method has significantly lower standard deviation of the histogram value than the values obtained by the post-processing methods within each fill factor value, indicating significantly more preservation of original information; thirdly our method has significantly less variation of standard deviation of the histogram values having different fill factors in comparison to the results from the post-processing methods; indicating the distinguish between recordable and displayable properties of the methods.

Table 3. The standard deviation of the histogram distribution.

Fill Factor	Our method	Histogram equalization	Image enhancement
25%	72.25	183.52	178.41
36%	68.87	153.59	140.54
49%	74.41	142.62	123.99
64%	74.35	131.21	104.08
81%	74.91	124.72	88.95

6 Conclusion

In this paper, a novel software-based method is proposed for widening the dynamic range in CCD sensor images by increasing the fill factor virtually. The experimental results show that the low fill factor causes high RMSE and low dynamic range in conventional sampling images and increase of fill factor causes increase of dynamic range. Also the results show that 100% fill factor can be achieved by our proposed method; obtaining low RMSE and high dynamic range. In the proposed method, a

CCD image and a known value of fill factor are used to generate virtual pixels of the CCD sensor where the intensity value of each pixel is estimated by considering an increase of fill factor to 100%. The stability and fill factor dependency of the proposed method were examined in which the results showed a maximum of 1.6 in RMSE and 0.02 in entropy of all resampled images for standard deviation in comparison to the optical image from the proposed method and fill factor dependency was insignificant. In the future works we will apply our methodology on CMOS sensors and the color sensors.

References

1. Prakel, D. The Visual Dictionary of Photography. AVA Publishing, 91. ISBN 978-2-940411-04-7 (2013)
2. Curcio, C.A., Sloan, K.R., Kalina, R. E., Hendrickson, A. E. Human photoreceptor topography. J. Comp. Neurol, 292, 497–523 (1990)
3. Rossi, E.A., Roorda, A. The relationship between visual resolution and cone spacing in the human fovea. Nat Neurosci, 13:156–157 (2010)
4. Goldstein, D.B. Physical Limits in Digital Photography http://www.northlight-images.co.uk/article_pages/guest/physical_limits_long.html (2009)
5. Burke, B., Jorden, P., Vu, P. CCD Technology, Experimental Astronomy, vol. 19, 69-102 (2005)
6. Chen, T., Catrysse, P., Gamal, A. E., Wandell, B. How small should pixel size be? Proc. SPIE, vol. 3965, 451–459 (2000)
7. Reinhard, E., Ward, G., Pattanaik, S. Debevec, P. High Dynamic Range Imaging: Acquisition,Display and mage-Based Lighting, Morgan Kaufmann Publishers, San Francisco, California, S.U.A (2005)
8. Yeganeh, H., Wang, Z. High dynamic range image tone mapping by maximizing a structural fidelity measure. In IEEE International Conference on Acoustics, Speech and Signal Processing, pp. 1879–1883 (2013)
9. Abdullah-Al-Wadud, M., et al, A Dynamic Histogram Equalization for Image Contrast Enhancement, IEEE Trans., Consumer Electronics, vol.53, no. 2, pp. 593 – 600, (2007)
10. Sebastiano, B., Arcangelo R.B., Giuseppe, M., Giovanni, P. Image Processing for Embedded Devices: From CFA Data to Image/video Coding. Bentham Science Publishers. p. 12. ISBN 9781608051700 (2010)
11. Dalsa, Image sensor architectures for digital cinematography http://www.teledynedalsa.com/public/corp/PDFs/papers/Image_sensor_Architecture_Whitepaper_Digital_Cinema_00218-00_03-70.pdf (2003)
12. Deguchi, M., Maruyama, T., Yamasaki, F. Microlens Design using Simulation Program for CCD Image Sensor, IEEE Trans Consumer Electronics, 583-589. (1992)
13. Donati, S., Martini, G., Norgia, M. Microconcentrators to recover fill- actor in image photodetectors with pixel on-board processing circuits. Opt. Express 15, 18066–18075 (2007)
14. Potmesil, M., Chakravarty, I. Modelling Motion Blur in Computer-Generated Images. Computer Graphics, vol. 17, 3, 389-399 (1983)
15. Farrell, J., Xiao, F., Catrysse, P., Wandell, B. A simulation tool for evaluating digital camera image quality. In Proc. SPIE Int. Soc. Opt. Eng., vol. 5294, 124 (2004)
16. Farrell, J., Okincha, M., Parmar, M. Sensor calibration and simulation, In Proc. SPIE Int. Soc. Opt. Eng., vol. 6817 (2008)